Salt-Gel Synthesis of Porous Transition-Metal Oxides

Andreas Stein,*,† Mark Fendorf,§ Thomas P. Jarvie,‡ Karl T. Mueller,‡ Alan J. Benesi,‡ and Thomas E. Mallouk*,‡

Department of Chemistry, University of Minnesota, Minneapolis, Minnesota 55455; Department of Chemistry, Pennsylvania State University, University Park, Pennsylvania 16802; and Department of Chemistry, University of California, Berkeley, California 94720

Received August 2, 1994. Revised Manuscript Received November 21, 1994[⊗]

Hydrothermal reaction of sodium metatungstate with the surfactant template cetyltrimethylammonium (CTA) hydroxide gave the salt $(C_{19}H_{42}N)_6(H_2W_{12}O_{40})$. Despite the superficial similarity of TEM micrographs and powder X-ray patterns of this material to those of mesoporous silicates, the salt contains unconnected Keggin ions $H_2W_{12}O_{40}^{6-}$. These Keggin ions pack in a puckered layer arrangement and create roughly spherical cavities for the surfactant micelle counterions. Attempts to remove the template cations and condense the inorganic portion of the structure invariably lead to dense WO_{3-x} phases. $Nb_xW_{6-x}O_{19}^{(2+x)-}$ (x = 2, 3, 4) clusters also formed layered salts with CTA cations, which were reacted with tetraethyl orthosilicate (TEOS). The TEOS molecules are absorbed, presumably into the hydrophobic portion of the structure, and can be hydrolyzed to form silica within the salt. Infrared and solid-state NMR double-resonance spectra show that the silica network is anchored to the clusters via covalent Nb-O-Si linkages. Extraction of the silica-modified salts with HCl/ethanol yields materials with both micropores and mesopores and specific surface areas up to 265 m^2/g.

Introduction

The already large field of molecular sieve synthesis recently received another significant boost when the synthesis of the new mesoporous molecular sieves MCM-41 was described.[1,2] MCM-41 is a silica-based mesoporous structure with regularly arranged channels of 20-100 Å diameters. Its potential for catalyzing reactions of sizable organic molecules has been demonstrated.[3,4] The synthesis of MCM-41 involves the use of surfactants as structure-directing templates. The organic templates can be removed by calcination, leaving a channel system that is accessible to large molecules.

Since the initial announcement of MCM-41, several groups have successfully incorporated small amounts of other elements into the silicate structure, including Al and Ti.[2,5] Stucky, Schüth, and co-workers reported the generalized synthesis of periodic surfactant/inorganic composite materials using cationic and anionic surfactants and inorganic counterions, including tungsten, antimony, lead, iron, aluminum, and zinc species.[6] They observed hexagonal and lamellar tungsten oxide/surfactant composites. This work followed earlier studies of hydrothermally synthesized tungsten oxides with the hexagonal tungsten bronze and pyrochlore structures.[7]

We have independently explored the general applicability of the use of surfactants for the synthesis of channel structures with transition metal oxide frameworks. Vanadium, niobium, molybdenum, and tungsten oxides were studied. Our study showed that the tungsten oxide precursors do not form a condensed (connected) framework but instead aggregate to form thermodynamically stable Keggin ions. These precipitate with cationic surfactants as a salt. The arrangement of Keggin clusters results in a three-dimensional tunnel structure. Vanadium, niobium, and molybdenum form similar cluster ion salts, often with lamellar structures.[8]

Keggin ions are very stable species and show very little tendency to condense in the surfactant salt structures. Hence, any attempt at removing the organic "template" resulted in dense WO_{3-x} phases. To form a more connected framework, which can remain linked after the surfactant removal, we synthesized surfactant salts of more reactive niobotungstate clusters[9-12] and reacted these with tetraethyl orthosilicate (TEOS) in a "salt-gel" reaction. The principle of the "salt-gel" reaction is to transform a crystalline array of molecular

† University of Minnesota.
‡ Pennsylvania State University.
§ University of California.
⊗ Abstract published in *Advance ACS Abstracts,* January 1, 1995.

(1) Kresge, C. T.; Leonowicz, M. E.; Roth, W. J.; Vartuli, J. C.; Beck, J. S. *Nature* **1992**, *359*, 710.
(2) Beck, J. S.; et al. *J. Am. Chem. Soc.* **1992**, *114*, 10834.
(3) Le, Q. N.; Thomson, R. T.; Yokomiso, G. H. U.S. Patents 5,134,241 and 5,134,242, July 28, 1992.
(4) Bhore, N. A.; Le, Q. N.; Yokomiso, G. H. U.S. Patent 5,134,243, July 28, 1992.
(5) Tanev, P. T.; Chibwe, M.; Pinnavaia, T. J. *Nature* **1994**, *368*, 321.
(6) (a) Huo, Q.; et al. *Nature* **1994**, *368*, 317; (b) Alfredsson, V.; et al. *J. Chem. Soc., Chem. Commun.* **1994**, 921. (c) Ciesla, U.; et al. *J. Chem. Soc., Chem. Commun.* **1994**, 1387.
(7) (a) Reis, K. P.; Prince, E.; Whittingham, M. S. *Chem. Mater.* **1992**, *4*, 307. (b) Reis, K. P.; Ramanan, A.; Whittingham, M. S. *J. Solid State Chem.* **1992**, *96*, 31.
(8) Stein, A.; Mallouk, T. E., unpublished results.
(9) Day, V. W.; Klemperer, W. G. *Science* **1985**, *228*, 533.
(10) Day, V. W.; Klemperer, W. G.; Schwartz, C. *J. Am. Chem. Soc.* **1987**, *109*, 6030.
(11) Day, V. W.; Klemperer, W. G.; Schartz, C.; Wang, R.-C. In Basset, et al., eds. *Surface Organometallic Chemistry: Molecular Approaches to Surface Catalysis*; Kluwer Academic Publishers: Dordrecht, 1988; p 173.
(12) Dabbabi, M.; Boyer, M. *J. Inorg. Nucl. Chem.* **1976**, *38*, 1011.

0897-4756/95/2807-0304$09.00/0

or low-dimensional building blocks, which are not connected, into a fully connected three-dimensional array by adding a component that forms covalent links between them. The process resembles the sol–gel method, except that the precursor phase is already ordered via ionic and/or noncovalent interactions. Such a low-temperature solid-state reaction has been used previously to prepare molecular sieves from dense, layered metal oxides.[13]

We report here the syntheses and structural properties of the tungstate and niobotungstate surfactant salts as well as the corresponding TEOS-treated products of the salt–gel reactions.

Experimental Section

Synthesis of $(C_{19}H_{42}N)_6(H_2W_{12}O_{40})$. The tungstate/surfactant composites were synthesized by dissolving sodium metatungstate (Aldrich) in distilled water and adding the appropriate amount of an aqueous solution containing 26 wt % cetyltrimethylammonium hydroxide (CTAOH) to obtain surfactant-to-metal ratios from 0.015 to 0.5. The latter solution was obtained by batch ion exchange of cetyltrimethylammonium chloride (TCI) with Amberlite IRA-400(OH) ion-exchange resin (Rohm and Haas Co.). Immediately a white gel precipitated. This gel was allowed to react in Teflon-lined autoclaves at temperatures from 95 to 170 °C. During the reaction, the solution pH generally dropped from an initial value of pH 9 to a final value of pH 7. After reaction times from 24 to 96 h, the white solid products were collected by filtration and washed with distilled water. They were dried in air at 95 °C. The most crystalline product was obtained with a surfactant-to-metal ratio of 0.5 at 95 °C after 72 h reaction time. Chemical analysis: observed: C, 29.76%; H, 5.67%; N, 1.90%; calculated for $(C_{19}H_{42}N)_6(H_2W_{12}O_{40})$: C, 30.05%; H, 5.62%; N, 1.84%.

Synthesis of $(C_{19}H_{42}N)_4(Nb_2W_4O_{19})$. $(TMA)_4(Nb_2W_4O_{19})$ was synthesized according to the method described by Dabbabi et al.[12] An intimate mixture of 6.38 g of Nb_2O_5 (Aldrich) and 19.13 g of K_2CO_3 (Fisher) was fused at 1000 °C for 2 h in an alumina crucible. The melt was dissolved in 200 mL of deionized water, forming a $K_8Nb_6O_{19}$ solution. This solution was slowly added to 200 mL of a stirred 0.5 M sodium tungstate (Baker)/0.5 M H_2O_2 solution at 70 °C. The H_2O_2 was used to solubilize the Nb^V and to prevent Nb_2O_5 formation under the acidic reaction conditions.[14] After the pH was brought to 5.5 using glacial acetic acid (EM Science), the mixture was refluxed for 2 h. Concentrated sodium bisulfite (20 mL, Fisher) solution was added to destroy excess H_2O_2, followed by a solution of 7.11 g of tetramethylammonium (TMA) chloride (Aldrich) in 10 mL of deionized water. When the solution had cooled to room temperature, any precipitated solids were removed by filtration. When 500 mL of ethanol was added to the filtrate, a white precipitate of $(TMA)_4(Nb_2W_4O_{19})$ formed immediately. It was collected by filtration and dried in air. The IR spectrum of this product was identical to the published spectrum for $(TMA,Na,K)_4(Nb_2W_4O_{19})$.[15]

The cetyltrimethylammonium (CTA) salt was formed by dissolving 5.00 g of $(TMA)_4(Nb_2W_4O_{19})$ in 10.0 g of deionized water at 90 °C and adding this solution to a warm solution of 15.28 g of CTACl in 40.0 g of water. Immediately a precipitate formed. It was collected by filtration, after the solution had cooled to room temperature, and dried in air. Chemical analysis: observed: C, 37.80%; H, 7.16%; N, 2.26%; calculated for $(C_{19}H_{42}N)_4(Nb_2W_4O_{19})$: C, 38.62%; H, 7.16%; N, 2.37%.

Synthesis of $(C_{19}H_{42}N)_5(Nb_3W_3O_{19})$. An aqueous mixture of $K_8Nb_6O_{19}$ and Na_2WO_4/H_2O_2 was prepared as above. The pH was adjusted to a value of 8 by adding 15 mL of 6 M HCl. The solution was refluxed for 4 h to minimize the production of $Nb_4W_2O_{19}^{6-}$.[12] Na_2SO_3 (50 mL, 2 M Fisher) solution was added, the solution was cooled in an ice bath and filtered. Virtually no solids were present.

The filtrate was separated into two halves. A solution of 6.58 g of TMACl in 10 mL of water was added to one-half. A white precipitate formed immediately. It was filtered and dried in air. Its IR spectrum agreed with the published spectrum for $(TMA,Na,K)_5(Nb_3W_3O_{19})$.[12,15]

The cetyltrimethylammonium salt was formed by adding a solution of 19.2 g of CTACl in 50 mL of water to the other half of the filtrate. The precipitate that formed was collected by filtration, and dried in air. Chemical analysis: observed: C, 43.90%; H, 8.38%; N, 2.68%; calculated for $(C_{19}H_{42}N)_5(Nb_2W_4O_{19})$: C, 44.62%; H, 8.28%; N, 2.73%; calculated for $(C_{19}H_{42}N)_{4.87}Na_{0.13}(Nb_2W_4O_{19})$: C, 44.04%; H, 8.17%; N, 2.70%.

Synthesis of $(C_{19}H_{42}N)_6(Nb_4W_2O_{19})$. An aqueous mixture of $K_8Nb_6O_{19}$ and Na_2WO_4/H_2O_2 was prepared as above. The pH was adjusted to a value of 8 by adding 15 mL of 6 M HCl. The solution was boiled for 10 min. Na_2SO_3 (50 mL, 2 M) solution was added, the solution was cooled in an ice bath. Needle-shaped crystals of $(Na,K)_6(Nb_4W_2O_{19})$ formed overnight.[12] The IR spectrum agreed with the literature spectrum.[15]

$(C_{19}H_{42}N)_6(Nb_4W_2O_{19})$ formed as a white precipitate when an aqueous solution of $(Na,K)_6(Nb_4W_2O_{19})$ (0.65 g in 10 mL of water) was added to a CTACl solution (1.00 g in 10 mL of water).

Synthesis of the Protonated Niobotungstate Salts. Partially protonated niobotungstate salts were synthesized following a procedure by Day et al. for similar salts with smaller organic counterions.[10] A solution of 0.4 mL of THF containing a 4-fold mole excess of chloroacetic acid (Aldrich) was added to a rapidly stirred slurry of 1 g of $(C_{19}H_{42}N)_{4+n}(Nb_{2+n}W_{4-n}O_{19})$ (n = 0–2) in 6 mL of THF. Stirring was continued for 1–2 days at room temperature. The products were washed with THF and ether. IR spectra of the protonated salts did not differ from the unprotonated salts, but chemical analysis for C, H, and N indicated that partial exchange had occurred (e.g. $(C_{19}H_{42}N_3)_{3.54}(Nb_2W_4O_{19}H_{0.46})$).

Reaction with Tetraethyl Orthosilicate (TEOS). Silicate was introduced into the salts by reacting 1.0 g of the cluster/surfactant salt with 1.0 g (excess) of TEOS (Aldrich) at 160 °C for 24 h. This reaction was carried out in a Teflon-lined steel autoclave. The product was collected by filtration, washed with 95% ethanol, and dried in air.

Ammonium Chloride Wash. Several TEOS-treated samples were subsequently immersed in 4 M aqueous NH_4Cl (EM Science) solution (4 h, room temperature) to promote the hydrolysis process further. The products were separated by decanting, washed with water, and dried in air.

Extraction of Template. The cationic surfactant was removed by stirring ca. 0.5 g of the TEOS-treated Keggin salt in 150 mL of 1 M HCl/EtOH (Alfa) at room temperature for 24 h. The product was collected by filtration, washed with ethanol, and dried in air.

Product Characterization. Chemical analyses for C, H, and N were carried out by Atlantic Microlab, Inc., Norcross, GA. The water content of some samples was determined using a DuPont 951 thermogravimetric analyzer. Powder densities were determined with a Micromeritics Model 1305 multivolume pycnometer. X-ray patterns of the powders were collected using a Philips Model PW-1011/60 automated powder diffractometer with Cu Kα radiation and a nickel filter. They were analyzed using Scintag software. Fourier transform infrared spectra were collected on a Perkin-Elmer 1600 Series FTIR spectrometer, using KBr pellets of the samples. UV–visible diffuse reflectance spectra were obtained using a Varian DMS300 UV–visible spectrophotometer with diffuse reflectance accessory. Nitrogen BET surface area and pore size measurements were carried out using a Micromeritics ASAP2000 instrument.

(13) (a) Landis, M. E.; Aufdembrink, B. A.; Chu, P.; Johnson, I. D.; Kirker, G. W.; Rubin, M. K. *J. Am. Chem. Soc.* **1991**, *113*, 3189. (b) Inagaki, S.; Fukushima, Y.; Kuroda, K. *J. Chem. Soc., Chem. Commun.* **1993**, 680.

(14) Finke, R. G.; Droege, M. W. *J. Am. Chem. Soc.* **1984**, *106*, 7274.

(15) (a) Rocchiccioli-Deltcheff, C.; Thouvenot, R.; Dabbabi, M. *Spectrochim. Acta* **1977**, *33A*, 143. (b) Rocchiccioli-Deltcheff, C.; Thouvenot, R.; Franck, R. *Spectrochim. Acta* **1976**, *32A*, 587.

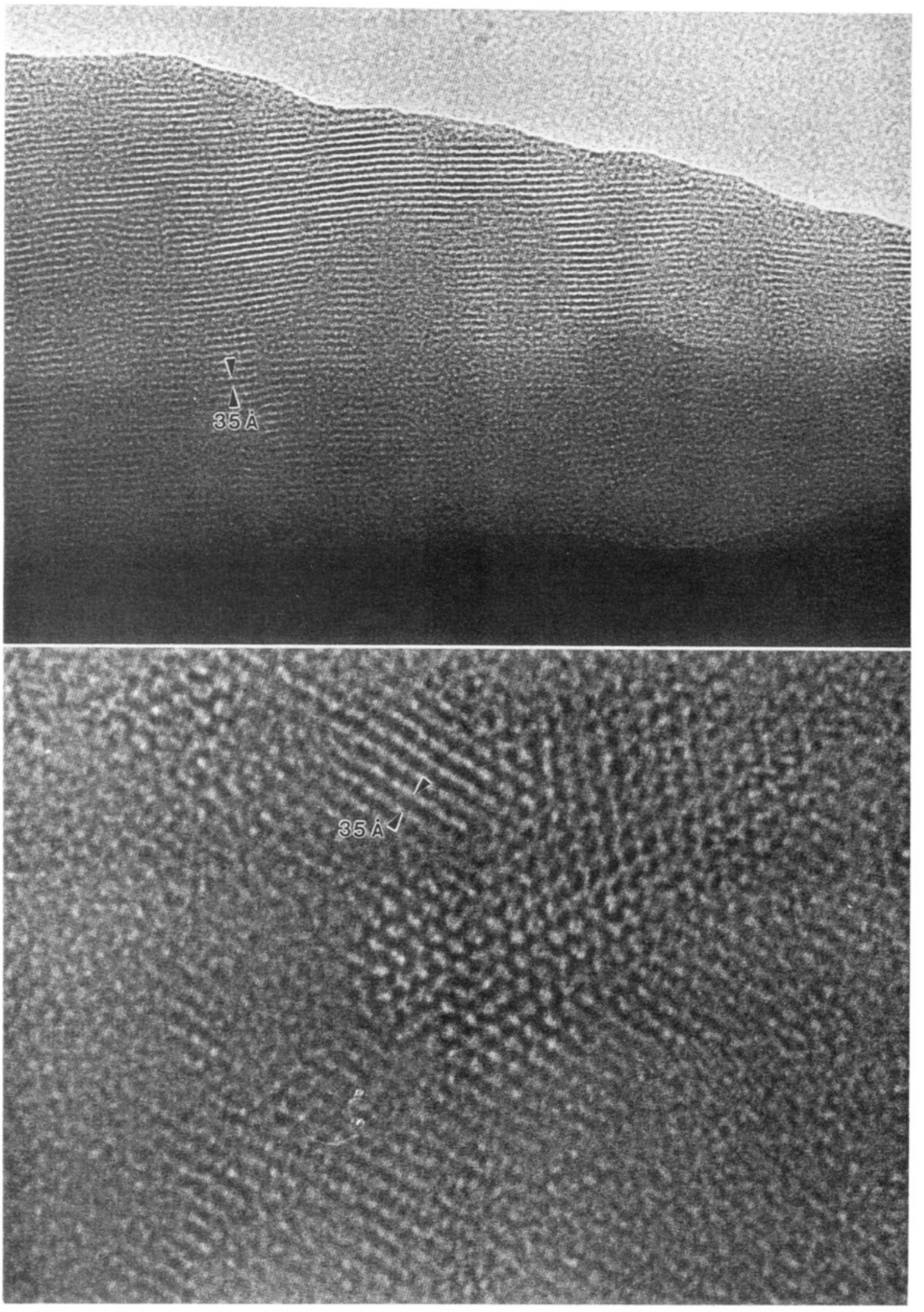

Figure 1. Transmission electron micrographs of $(C_{19}H_{42}N)_6(H_2W_{12}O_{40})$, showing parallel layers of the pseudohexagonal phase viewed at right angles to the *b* axis (top), and pseudohexagonal regions viewed along the *b* axis (bottom).

Specimens were prepared for TEM examination by crushing the starting materials to a fine powder and dispersing the resulting particles on a holey carbon film supported by a copper mesh grid. High-resolution electron microscopy was carried out using a Hitachi H-9000NAR microscope operating at 300 kV and a Topcon 002B operating at 200 kV. Both microscopes were equipped with a lanthanum hexaboride (LaB_6) filament.

Cross-polarization magic-angle spinning (CPMAS) ^{29}Si NMR spectra were collected on a Chemagnetics CMX-300 spectrometer (^{29}Si resonance 59.075 MHz) with a Chemagnetics Pencil probe, and both single-pulse MAS and dipolar-dephasing difference double-resonance[16] MAS spectra were acquired on a home-built 400 MHz spectrometer (^{29}Si resonance 79.461 MHz) based on a Tecmag system with a home-built MAS

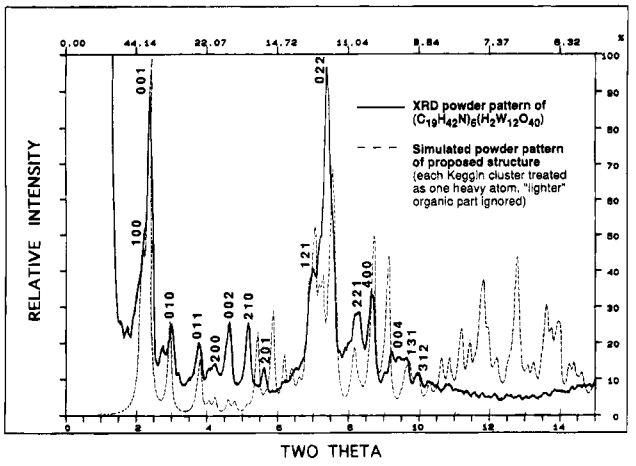

Figure 2. X-ray powder pattern of $(C_{19}H_{42}N)_6(H_2W_{12}O_{40})$ (solid line), and a simulated powder pattern (dashed line), based on the approximate model described in the text.

probe. In the dipolar-dephasing difference experiment, ^{29}Si spin echoes are acquired both with and without irradiation of the ^{93}Nb nucleus at 97.900 MHz. The difference spectrum shows only those resonances from ^{29}Si nuclei near to ^{93}Nb nuclei. ^{29}Si chemical shifts were referenced to TMS (0 ppm) indirectly with the secondary reference standards tetrakis(trimethylsilyl)silane at 59 MHz (peaks at −9.8 and −135.4 ppm) and zeolite A at 79 MHz (peak at −89.6 ppm). All spectra were recorded with spinning speeds between 3 and 4 kHz.

Results and Discussion

Surfactant/Keggin Salt. Figure 1 shows transmission electron micrographs of the tungstate structure with the occluded surfactant templates. Regularly spaced (35 Å) parallel layers are seen in Figure 1a, many of which continue through the length of the particle and terminate at the particle surface. The dark areas correspond to tungstate regions with thicknesses of approximately 15–20 Å, and the light areas to regions of similar dimensions occupied by the organic templates. A few defects exist, where the layers are bent or blocked. More than one layer spacing can be seen, probably as a consequence of imaging different crystal orientations. Figure 1b demonstrates a pseudohexagonal arrangement of channels down the unique *b* direction. The channels appear to be ellipsoidal, resulting in a monoclinic unit cell. The observed X-ray powder pattern (Figure 2) could also be indexed to a monoclinic unit cell with dimensions $a = 47.5$ Å, $b = 30.3$ Å, $c = 43.6$ Å, $\beta = 118°$. While the diffraction lines are sharp at low angles, the XRD pattern shows broad lumps at angles greater than 20° 2θ. These features are again reminscent of MCM-41, which shows sharp low-angle lines and diffuse high-angle lines, indicative of long-range ordering of channels but a locally glassy aluminosilicate framework.[2] The electron micrographs obtained in our experiments resemble those given by Stucky, Schüth, et al.,[6] even though their tungsten oxide/surfactant composites were prepared under slightly more acidic conditions, which tend to favor condensation. We found that similar products were obtained under a wide range of temperature, concentration, and pH conditions, whether the starting material was sodium tungstate or sodium metatungstate.

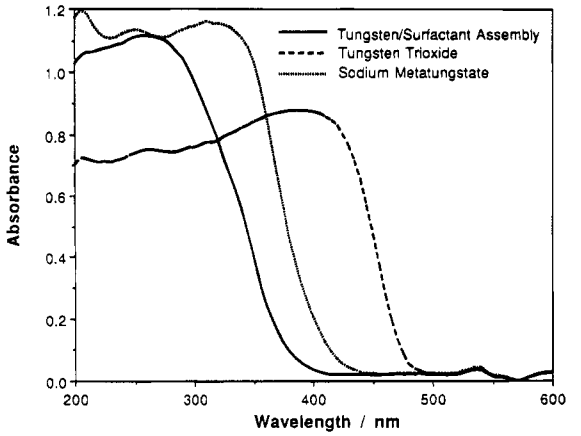

Figure 3. UV–visible diffuse reflectance spectra of $(C_{19}H_{42}N)_6(H_2W_{12}O_{40})$, WO_3, and $3Na_2WO_4{\cdot}9WO_3{\cdot}xH_2O$.

While the TEM micrographs in Figure 1 show regions that resemble the micrographs of the MCM-41 channel structure, and the unit cell determined by XRD is consistent with an open structure like that of mesoporous silicates, several other properties of the tungstate/surfactant composites indicate that the inorganic components do not form a connected framework.

UV–visible absorption spectra of the tungstate/surfactant assembly, bulk tungsten trioxide, and sodium metatungstate are shown in Figure 3. The absorption edge for the assembly is blue-shifted from bulk tungsten trioxide, as one would expect for a spatially confined metal oxide. Its blue shift with respect to sodium metatungstate is unexpected. It indicates the presence of more isolated metal oxide units, such as Keggin clusters, which are separated from each other by a greater distance than in sodium metatungstate.

The infrared spectrum of the tungstate/surfactant composite exhibits several strong W–O stretching vibrations in the region between 1000 and 700 cm^{-1}. It closely resembles the pattern observed for sodium metatungstate, showing the typical features of $H_2W_{12}O_{40}^{6-}$ Keggin anions,[15b] but it is very different from the IR spectrum of $Na_2WO_4{\cdot}2H_2O$ (with WO_4^{2-} tetrahedra) or that of WO_3 (a condensed tungsten oxide network) (Figure 4). Following the assignments of Rocchiccioli-Deltcheff et al.,[15b] we assign the strong resonances at 770 and 878 cm^{-1} to the ν(M–O–M) vibration and a peak at 929 cm^{-1} with a shoulder at 950 cm^{-1} to the $\nu(M{-}O_t)$ vibration (O_t refers to a terminal oxygen). The shoulder at 962 cm^{-1} coincides with Rocchiccioli-Deltcheff's assignment for ν(OH) in the $H_2W_{12}O_{40}^{6-}$ cluster.

The chemical analysis of the tungstate/surfactant composite is consistent with the composition $(C_{19}H_{42}N)_6(H_2W_{12}O_{40})$. Given a measured density of 2.0 g cm^{-3} and the unit-cell volume obtained from the powder pattern (see below), one would obtain a wall thickness of 3.3 Å if a connected tungsten oxide framework were present in this system. This thickness is inconsistent with the TEM observations and much smaller than that found in MCM-41[17] (ca. 8–9 Å).

The combined above information provides convincing evidence that rather than forming a connected tungsten

(16) (a) van Eck, E. R. H.; Janssen, R.; Maas, W. E. J. R.; Veeman, W. S. *Chem. Phys. Lett.* **1990**, *174*, 428. (b) Fyfe, C. A.; Mueller, K. T.; Grondey, H.; Wong-Moon, K. C. *J. Phys. Chem.* **1993**, *97*, 13484.

(17) Monnier, et al. *Science* **1993**, *261*, 1299.

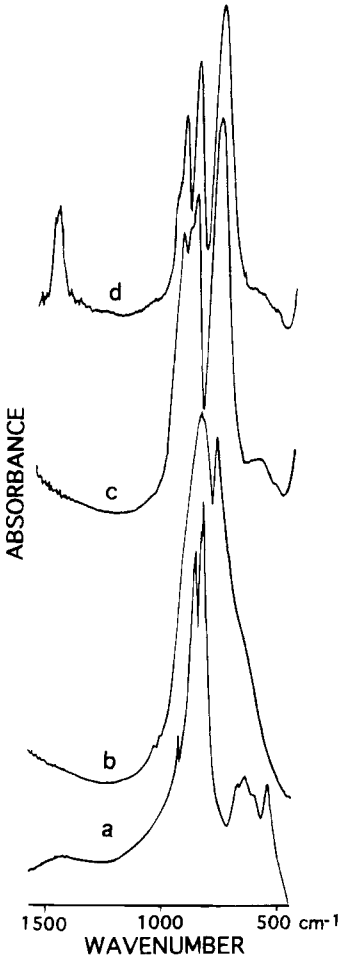

Figure 4. Infrared spectra of (a) $Na_2WO_4 \cdot 2H_2O$, (b) WO_3, (c) $3Na_2WO_4 \cdot 9WO_3 \cdot wH_2O$ (sodium metatungstate), and (d) $(C_{19}H_{42}N)_6(H_2W_{12}O_{40})$.

oxide framework around cylindrical or lamellar surfactant micelles, the tungstate/surfactant composite is a salt array of cationic surfactant molecules around quasi-spherical Keggin clusters (10−11 Å diameters[18]). The Keggin structure of α-$(XM_{12}O_{40})^{n-}$ has overall T_d symmetry and consists of a central XO_4 tetrahedron surrounded by 12 MO_6 octahedra that are arranged in four groups of three edge-shared octahedra[18] (Figure 5). In our case, protons occupy the central vacancy. Similar salts have been precipitated from solutions containing tetraalkylammonium cations and Keggin anions.[19,20]

A model for the structure of the surfactant/Keggin salt was developed, based on the monoclinic X-ray diffraction (XRD) powder pattern, the TEM image of a thin salt layer, and the composition/density information of the sample. The low-angle region of the X-ray powder pattern was simulated using the *X-Ray Diffraction Powder Generation Package POWD12*,[21] testing a large number of reasonable structures. In the simulation, each Keggin cluster was treated as one heavy atom, and the "lighter" organic part was ignored. Models with one to six layers along the unique *b* axis in the unit cell were tested. The cluster positions were optimized manually

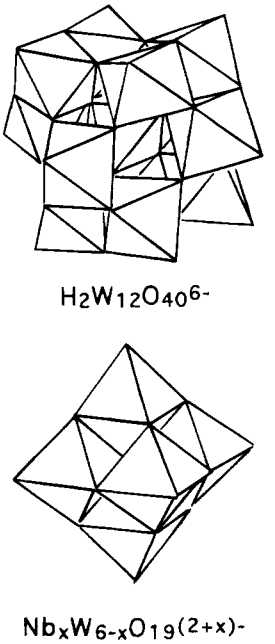

Figure 5. Polyhedral representations of $H_2W_{12}O_{40}^{6-}$ and $Nb_xW_{6-x}O_{19}^{(2+x)-}$ (adapted from Pope[18]).

Table 1. Coordinates of the Metatungstate Clusters in the Proposed Model Structure of $(C_{19}H_{42}N)_6(H_2W_{12}O_{40})$, Based on a Monoclinic Cell with a = 47.45 Å, b = 30.30 Å, c = 43.60 Å, and β = 118.24°

cluster	*x*	*y*	*z*
W1	0.500	0.000	0.000
W2	0.000	0.000	0.500
W3	0.500	0.000	0.500
W4	0.325	0.250	0.675
W5	0.675	0.250	0.325
W6	0.150	0.500	0.850
W7	0.500	0.500	0.150
W8	0.150	0.500	0.500
W9	0.500	0.500	0.500
W10	0.850	0.500	0.500
W11	0.500	0.500	0.850
W12	0.850	0.500	0.150
W13	0.325	0.750	0.675
W14	0.675	0.750	0.325

to obtain the best match with both the X-ray intensities and the TEM image. Our best model is shown in Figure 6. It consists of four layers along the *b* axis, arranged in the pattern ABCB (see Table 1). With this arrangement, large ellipsoidal channels appear down the *b* axis. One can note two clusters protruding into the large channels. These had to be included in the simulation in order to obtain the intense 220/202/022 reflections that were observed. By careful examination of the TEM photographs, one can observe weak protrusions into the channels. These clusters may serve to stabilize the surfactant micelles in the channels by forming pseudo-cages.

The view along the 101-direction reveals alternating layers of clusters and surfactants which resemble the layer lines observed on the TEM image. In our proposed model, individual Keggin clusters interrupt the surfactant layers every 30 Å, leading to an undulation in the Keggin layers. Such undulations can also be observed in several regions on the TEM pattern, providing further support to the model for the Keggin/surfactant salt. From this model one can conclude that the observation of both pseudohexagonal regions and layered regions in the TEM image results not from two different phases

(18) Pope, M. T. *Heteropoly and Isopoly Oxometalates*; Springer-Verlag: Berlin, 1983.
(19) Evans, H. T., Jr. *Perspec. Struct. Chem.* **1971**, *4*, 1.
(20) Smit, J. van R. *Nature* **1958**, *181*, 1530.
(21) Smith, D. K.; Johnson, G. G. Jr.; Scheible, A. *X-Ray Diffraction Powder Generation Package POWD12*; Vax Version, Nov 24, 1993, Materials Research Laboratory, Pennsylvania State University.

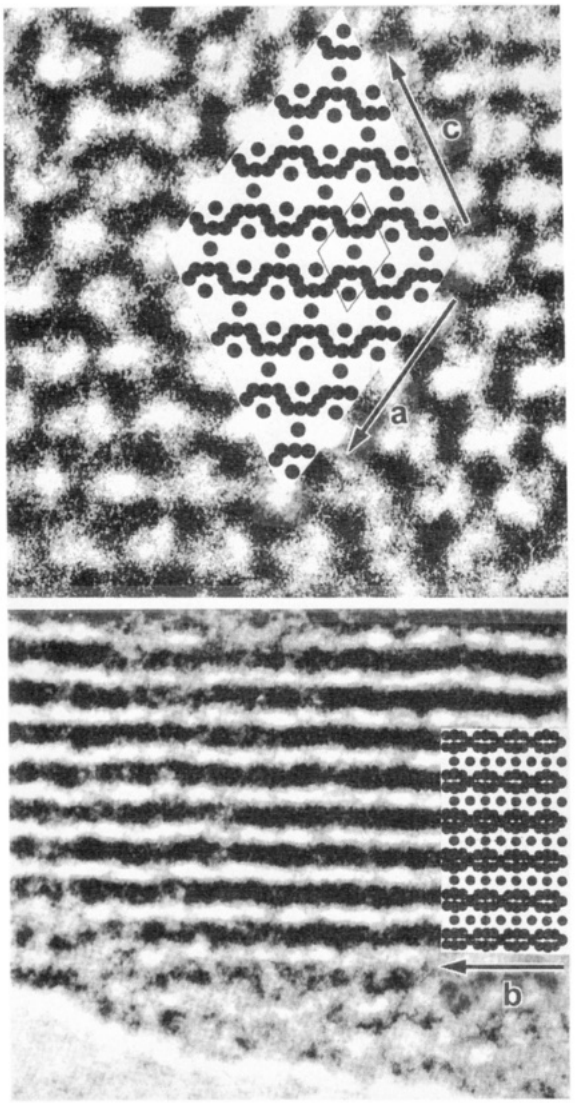

Figure 6. Simulated structures of $(C_{19}H_{42}N)_6(H_2W_{12}O_{40})$ superimposed on the corresponding TEM views. Top: view down the unique *b* axis. The monoclinic unit cell is outlined in the simulation. Bottom: view down the 101 direction, showing layers, spaced ca. 35 Å apart.

but from viewing the Keggin–surfactant salt along different crystallographic axes.

In the case of mesoporous silicates of the MCM-41 type, the long-range order of the oxide arrangement depends in part on the surfactant concentration.[17] A hexagonal phase is favored at low surfactant concentrations, while lamellar phases form at high concentrations. The spacings and channel diameters can be strategically controlled by the length of the surfactant. The situation changes for surfactant salts of Keggin ions. While the dimensions of the Keggin salt are still expected to depend on the hydrocarbon chain length, a wide range of surfactant concentrations can lead to the observed structure for a given surfactant. In the Keggin/surfactant gel, the cooperative forces between cations and anions become even more significant than in the silicate gels, due to the high charge on a Keggin ion and the strong association of the surfactant molecules with a specific Keggin ion.

Even though transition-metal clusters, such as Keggin ions, can be arranged into periodic arrays with giant tunnel structures, they would become useful mesoporous molecular sieve structures only if the surfactant could be eliminated, and hollow channel or cage structures with high surface areas would remain. With the surfactant present, the Keggin salts exhibit a very low surface area (ca. 1 m^2/g), as has been observed for other alkylammonium salts of heteropolytungstates.[22,23] We have found that surfactant-removal by heat treatment above 250 °C in vacuum, air, or oxygen yields the dense WO_{3-x} structure. Surfactant-extraction methods, such as acid leaching with ethanolic HCl, also lead to the collapse of the tunnel structures, essentially because the Keggin ions are not connected to each other and exhibit little tendency to condense under these conditions.

Niobotungstate Salt–Gels. To overcome the lack of cluster connectivity, we explored a new strategy that uses prearranged surfactant salt structures as precursors that can be bridged to form microporous and mesoporous framework materials. We studied silicates derived from tetraethyl orthosilicate (TEOS) as possible bridging candidates. The highly inert metatungstate clusters were replaced by more reactive niobotungstate clusters (Figure 5). Even though heteropolytungstate has been shown to react with alkylsilyl groups,[24] a study by Day et al.[9–11] comparing the reactivity of $W_6O_{19}^{2-}$ to niobium-substituted clusters indicated that the pure tungsten cluster is very nonbasic and unreactive toward many good electrophiles. Substitution of one or more W^{VI} sites by lower-valent Nb^V atoms produces reactive sites at both the terminal ONb oxygens and the bridging oxygens.[9] These workers were able to functionalize niobotungstic acid to form silyl esters. The strategy presented here involves the formation of niobotungstate/surfactant salts with a prearranged structure, bridging of the clusters with silicate groups, followed by removal of the surfactant to form a porous structure. Niobium oxosilicate linkages have been found in structures such as $Ba_3Nb_6Si_4O_{26}$,[25,26] $K_6Nb_6Si_4O_{26}$,[25] $Ba_3Nb_7Si_2O_{25-x}$,[27] $Ba_3Nb_{21-x}Si_2O_{44}$,[27] and $Ba_6Nb_{14}Si_4O_{47}$.[28] In these compounds mixed frameworks are built up from chains of corner- and/or edge-sharing NbO_6 octahedra and SiO_4 tetrahedra or Si_2O_7 groups.

$Nb_xW_{6-x}O_{19}^{(2+x)-}$ clusters ($x = 2, 3, 4$) were synthesized following the method described by Dabbabi and Boyer.[12] We will abbreviate these clusters Nb_2W_2, Nb_3W_3, and Nb_4W_2, respectively. To confirm their identity, the tetragonal tetramethylammonium salts were prepared first and analyzed by FTIR spectroscopy. The spectra obtained agreed with those found by Dabbabi et al.[15] All three of these anions ($x = 2, 3, 4$) precipitated readily with cetyltrimethylammonium to form white salts. The XRD powder patterns of the surfactant salts are shown in Figure 7a. They indicate good crystallinity (especially for $x = 2$) and significant layering, with some additional structure between the layers (weaker lines). The layering is also manifested in the TEM micrograph (Figure 8).

In the case of the niobotungstate anions, a pseudohexagonal phase like that found for the surfactant/Keggin

(22) McMonagle, J. B.; Moffat, J. B. *J. Colloid Interface Sci.* **1984**, *101*, 479.
(23) McMonagle, J. B.; Moffat, J. B. *J. Catal.* **1985**, *91*, 132.
(24) Ammari, N.; Hervé, G.; Thouvenot, R. *New J. Chem.* **1991**, *15*, 607.
(25) Choisnet, J.; Nguyen, N.; Raveau, B.; Gabelica-Robert, M.; Tarte, P. *J. Solid State Chem.* **1978**, *26*, 83.
(26) Shannon, J. R.; Katz, L. *Acta Crystallogr.* **1970**, *B26*, 105.
(27) Evans, D. M.; Katz, L. *J. Solid State Chem.* **1973**, *6*, 459.
(28) Serra, D. L.; Hwu, S.-J. *J. Solid State Chem.* **1992**, *101*, 32.

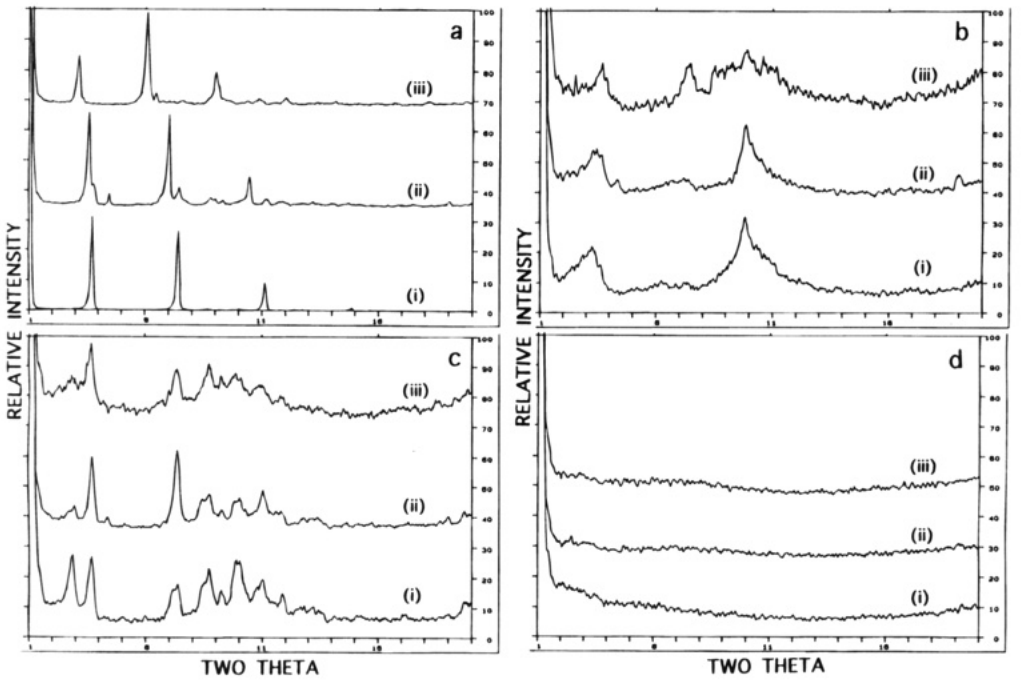

Figure 7. X-ray powder patterns of (a) the untreated surfactant/niobotungstate salts, (b) the TEOS-treated samples, (c) the TEOS-treated and NH_4^+-washed samples, and (d) the acid-extracted samples. For each case, patterns are shown for (i) $Nb_2W_4O_{19}^{4-}$, (ii) $Nb_3W_3O_{19}^{5-}$, and (iii) $Nb_4W_2O_{19}^{6-}$.

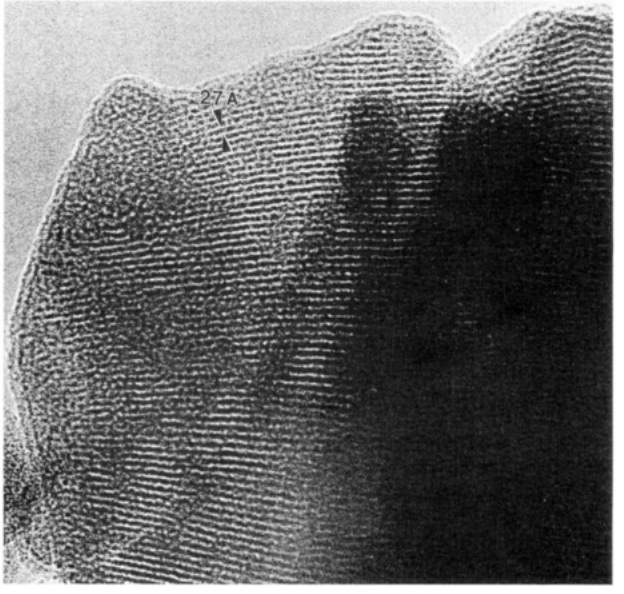

Figure 8. Electron micrograph of $(C_{19}H_{42}N)_4(Nb_2W_4O_{19})$ showing the layer structure of the lamellar phase before modification with TEOS and acid extraction.

salt was not observed. The major layer spacing in the X-ray diffraction pattern increased from 23.8 ± 0.1 to 25.0 ± 0.3 to 29.0 ± 0.6 Å as the negative charge on the cluster ion increased from −4 to −5 and −6 for Nb_2W_4, Nb_3W_3, and Nb_4W_2. The higher charge is compensated by more surfactant cations, which must pack more densely, resulting in the greater layer spacing. On the basis of CPK modeling, a fully extended CTA ion has a length of 24 Å; completely coiled up it extends ca. 12 Å. As the niobotungstate cluster size is ca. 8 Å, a space of ca. 16−21 Å is left for the organic groups. This implies that the hydrocarbon tails penetrate each other, as might be expected.

The difference in structures between the Keggin salt and the various niobotungstate salts may in part be related to the charges of these anions. The size difference of these anions is relatively small. Keggin anions typically have diameters between 10 and 11 Å,[18] while the diameters of niobotungstate clusters lie around 8 Å.[19] The salts of all three clusters are more strongly layered than the Keggin salt. However, both the Nb_3W_3 (charge −5) and the Nb_4W_2 (charge −6) salt show weak additional reflections, which are uniformly spaced and can be indexed as $0k0$ lines (and $00l$ lines in the case of Nb_3W_3). This may indicate additional structure between the layers. (A chemical analysis showed that the additional lines cannot be due to minor phases with mixed $CTA^+/Na^+/K^+$ counterions, as the alkali ion content is too low to account for the observed X-ray intensities.)

An oxolation reaction (a condensation reaction in which an oxo bridge is formed[29] between an Nb and an Si center) was attempted by heating a slurry of the surfactant salt in TEOS. TEOS can be absorbed into the organophilic region of the surfactants, akin to the process observed in layered metal oxides (alkali titanates) and silicates (magadiite, $Na_2Si_7O_{15}$, and kenyaite, $K_2Si_{14}O_{29}$).[13] A similar process has been used for the stabilization of MCM-41.[30] After thorough washing with ethanol, the TEOS-treated products are still white or off-white, indicating that the oxidation state of the cluster has not changed. These clusters contain only d^0 metal centers and are poor oxidizing agents.[31] (The TEOS-treated samples will be denoted as Si−Nb_2W_4, Si−Nb_3W_3, and Si−Nb_4W_2.)

Treatment of the cluster salts with TEOS resulted in powder patterns that generally showed broader reflections, less layering (i.e., more three-dimensional fea-

(29) Brinker, C. J.; Scherer, G. W. *Sol-Gel Science*; Academic Press: Boston, 1990.
(30) McCullen, S. B.; Vartuli, J. C. U.S. Patent 5,156,829, Oct 20, 1992.
(31) Dabbabi, M.; Boyer, M.; Jaunay, J. P.; Jeannin, Y. *J. Electroanal. Chem.* **1977**, *76*, 153.

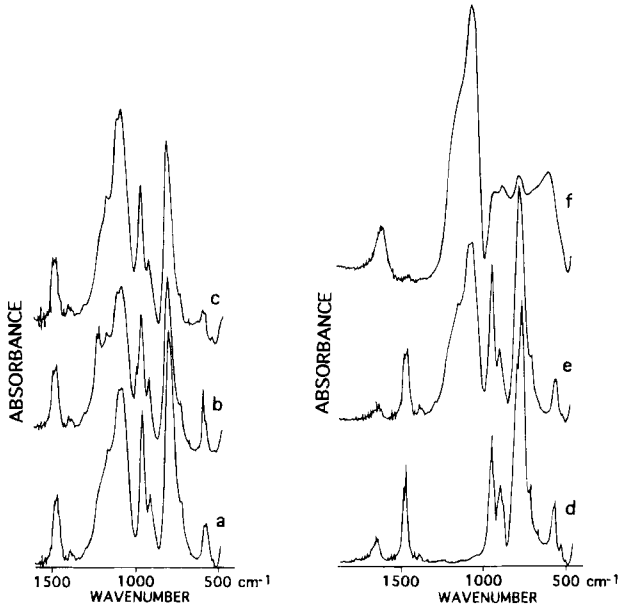

Figure 9. Infrared spectra of (a) Si–Nb_2W_4, (b) Si–Nb_3W_3, (c) Si–Nb_4W_2, (d) $(C_{19}H_{42}N)_4(Nb_2W_4O_{19})$, (e) Si–$Nb_2W_4$, and (f) acid-extracted Si–Nb_2W_4.

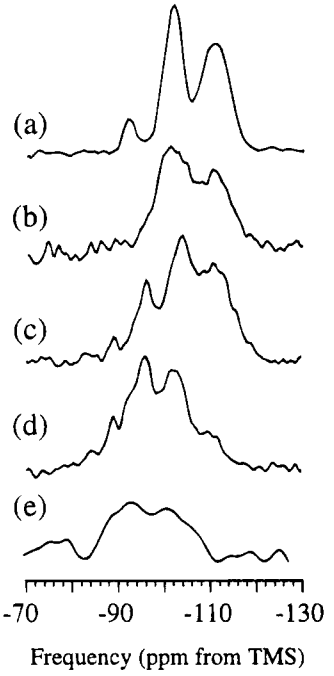

Figure 10. (a) ^{29}Si MAS NMR spectrum of TEOS-derived gel acquired with no CP or proton decoupling (spectrum adapted from Vega and Scherer[32]). Below are ^{29}Si CPMAS NMR spectra of (b) TEOS-treated $(C_{19}H_{42}N)_6(H_2W_{12}O_{40})$, (c) Si–$Nb_2W_4$, and (d) Si–$Nb_3W_3$ acquired with proton decoupling at 59.075 MHz. (e) The dipolar-dephasing $^{29}Si/^{93}Nb$ double-resonance MAS difference spectrum of Si–Nb_2W_4, acquired without cross-polarization or proton decoupling, at a ^{29}Si resonance frequency of 79.461 MHz.

tures) and a strong, broad reflection centered around 9 Å (Figure 7b). At reaction temperatures below 160 °C and reaction times less than 1 day, the conversion of the layered structure was incomplete. It is interesting to note that the order of the major spacing reversed for the series Nb_2W_4, Nb_3W_3, and Nb_4W_2 to 26.9, 25.4, and 24.0 Å, respectively, i.e., the spacing between layers increased for Nb_2W_4, remained unchanged for Nb_3W_3 and decreased for Nb_4W_2.

The FTIR spectra, shown in Figure 9, display new strong absorptions at ca. 1074–1098, 1105, and 1168 cm^{-1} and a shoulder at ca. 1220 cm^{-1} (resolved as two peaks at 1212 and 1228 cm^{-1} in case of the Nb_3W_3 sample). These are associated with the Si–O stretching vibrations of the silicate linkages. Choisnet et al. studied the IR vibrations of $K_6Nb_6Si_4O_{26}$ and $Ba_3Nb_6Si_4O_{26}$, which contain Si–O linkages between niobate clusters.[25] They found an effect of the local environment on the antisymmetric stretching frequency of linear Si–O–Si. (For example, in $K_6Nb_6Si_4O_{26}$ the antisymmetric ν_{as}(SiOSi) mode occurs at 1102 cm^{-1}.) In our samples, the absorption peak in the region from 1074 to 1098 cm^{-1} varied in wavenumber depending on the identity of the niobotungstate cluster and on the presence or absence of the surfactant. (TEOS/surfactant salts: Nb_2W_4, 1086; Nb_3W_3, 1078; Nb_4W_2, 1078 cm^{-1}. After HCl extraction: Nb_2W_4, 1098; Nb_3W_3, 1078; Nb_4W_2, 1074 cm^{-1}.) This effect suggests an association of the silicate units with the clusters, i.e., the possibility of Si–O–Nb bonds. The IR pattern of the niobotungstate cluster in the region below 1000 cm^{-1} remained virtually unperturbed. An absorption at 1394 cm^{-1} due to a C–H deformation mode indicates the presence of some remaining ethyl groups attached to silicon. It implies incomplete condensation of the silicate groups.

^{29}Si NMR spectra of the TEOS-treated samples were obtained, in order to determine whether Nb–O–Si linkages had actually formed. The spectra are shown in Figure 10, together with a spectrum of silica gel derived from TEOS.[32] All spectra reveal a Q^4 resonance at −110 ppm vs TMS due to SiO_4 surrounded by four other Si atoms. The observation of Q^4 resonances indicates that linkages longer than one silicate unit with other silicate side chains are present in the material. The presence of silicate chains and crosslinks between Nb_2W_4 clusters is further confirmed by the calculated SiO_2/Nb_2W_4 ratio of ca. 8–9 in the Nb_2W_4 sample.

The ^{29}Si NMR spectrum of the Si–W_{12} sample closely resembles that of unannealed silica gel. It shows two resonances at −110 ppm (Q^4) and −101 ppm (Q^3). In the case of the niobium-containing samples, the Q^2 (middle group) and Q^3 (2D-branching group) peaks shifted to higher field, similar to shifts observed when Si is replaced by Al. The Q^2 resonance was now found at −96 ppm (−91 ppm in silica gel), and the Q^3 resonance at −104 ppm (−101 ppm in silica gel). A weak Q^1 resonance (terminal group) was also shifted to higher field (−89 ppm compared to −82 ppm in silica gel).

The upfield shift of the Q^1, Q^2, and Q^3 resonances from silica gel can be interpreted in a number of ways. One possibility is the formation of Nb–O–Si bonds which would lead to the observed upfield shift. A second explanation for these resonances could be an incomplete hydrolysis product of TEOS, such as $Si(OH)_x(OEt)_{4-x}$ groups. In solution, hydrolysis of TEOS occurs rapidly, so that only peaks for $x = 4$ are observed.[32] In the salt–gel, hydrolysis could proceed more slowly, leading to the observation of mixed species whose resonances coincide with those found in the TEOS-treated Nb_2W_4 sample. However, we do not see any resonance due to unreacted TEOS, which would occur at −82 ppm.[32] A third

(32) Vega, A. J.; Scherer, G. W. *J. Non-Cryst. Solids* **1989**, *111*, 153.

possibility is the formation of TEOS dimers and trimers within the salt. These have chemical shifts at the same positions that we observed in the TEOS-treated Nb_2W_4 sample: TEOS dimer, $(Q^1)_2$ −88.85 ppm; trimer, $Q^1Q^2Q^1$ −99.99 for Q^1, −96.22 ppm for Q^2.[29]

The ambiguity of the ^{29}Si NMR data can be eliminated by carrying out a $^{93}Nb-^{29}Si$ double-resonance experiment. The dipolar-dephasing difference spectrum from $Si-Nb_2W_4$ (lower trace in Figure 10) shows considerable intensity in the region from −88 to −104 ppm, demonstrating that the observed ^{29}Si resonances in that region arise from ^{29}Si nuclei close enough to ^{93}Nb nuclei to experience a substantial spin dipole−dipole coupling. Since the dipolar interaction falls off as the third power of the internuclear distance, the observation of this signal is strong evidence for the formation of Nb−O−Si linkages. Shifts of the ^{29}Si resonances by 2 to 4 ppm were also detected as a function of the magnetic field strength, which also argues for the existence of a dipolar coupling between the spin $-^1/_2$ ^{29}Si nuclei and the quadrupolar ^{93}Nb spins.[33]

The relative ratios of Q^1, Q^2, Q^3, and Q^4 change between the samples with different cluster anions. The silicates in the $H_2W_{12}O_{40}^{6-}$ salt consist mostly of Q^3 and Q^4 units. In the Nb_2W_4 salt the Q^3 units predominate, while approximately equal amounts of Q^2 and Q^4 units are present. The Nb_3W_3 salt exhibits few Q^4 units. Mostly Q^2 and Q^3 groups are favored. This cluster has more reactive Nb sites than Nb_2W_4 and is therefore set up for more Q^2 bridges and more extensive cross-linking. Both sides of a Q^2 bridge may be connected to one cluster or may connect adjacent clusters.

Acid and Base Catalysis of Oxolation Reactions. Nb−O−Si linkages can be formed by a number of possible oxolation reactions. A hydrolysis step involving water as a reagent is required in each of these pathways. The water can come from trapped water in the crystal. TGA (of the Keggin salt) showed a water content of 1.3% or about one water molecule per CTA molecule. An infrared absorption at 1637 cm^{-1} corresponding to the H−O−H deformation mode indicates that water is present in the surfactant salts.

Water could hydrolyse the TEOS first, followed by reaction with the niobotungstate cluster (@-NbO) (eq 1) or it could react directly with the cluster (eqs 2 and 3).

$$Si(OH)_4 + @\text{-}NbO^- \rightarrow @\text{-}NbO{-}Si(OH)_3 + OH^- \quad (1)$$

$$Si(OEt)_4 + 4H_2O \rightarrow Si(OH)_4 + 4EtOH$$

$$Si(OEt)_4 + @\text{-}NbO^- \rightarrow @\text{-}Nb{-}O{-}Si(OEt)_3 + EtO^- \quad (2)$$

$$EtO^- + H_2O \rightarrow EtOH + OH^- \quad (3)$$

In both cases hydroxyl ions are produced, which can catalyze further condensation reactions:[29]

$$\equiv Si{-}OH + OH^- \xrightarrow{fast} \equiv Si{-}O^- + H_2O$$

$$\equiv SiO^- + HO{-}Si\equiv \xrightarrow{slow} \equiv Si{-}O{-}Si\equiv + OH^- \quad (4)$$

Condensation of silanols can proceed thermally without the use of an acid or base catalyst. However, employment of a catalyst can enhance the reaction kinetics, as better leaving groups are produced.[29] In the synthesis of glasses, the condensation of silicate groups is sensitive to the water content. The hydrolysis reaction can be performed with H_2O/Si ratios ranging from <1 to >25,[29] but it proceeds more rapidly with higher H_2O/Si ratios.[32] Since the water content in the Keggin salts is relatively low and difficult to control, we tested two methods to increase the opportunities for Nb−O−Si linking. Both involve the use of protons to neutralize EtO^- groups ($pK_a(EtOH) = 18$[34]) and drive the oxolation reaction to the product side. One uses a washing procedure of the TEOS-treated salts with NH_4^+ ($pK_a(NH_3) = 9.247$[34]), which is significantly more acidic than water. The second method is based on protonating the niobotungstate clusters before reacting the salt with TEOS.

The crystallinity of the samples treated with ammonium increased considerably. At the same time, the complexity of the low-angle reflections increased, indicating greater structure between the layer lines (Figure 7c). The acid extraction times required for template removal (see below) increased for these samples, possibly indicating greater cross-linking in these samples. Both chemical analyses and IR spectra of the ammonium-treated samples showed that CTA cations had not been replaced with ammonium ions during the treatment. The only difference from the spectra obtained for samples not exposed to ammonium ions is found in the relative intensities of the Si−O absorptions compared to the M−O absorptions, which decreased significantly after the treatment.

Another approach to improving the condensation of Nb−O−Si entailed the use of protonated niobotungstate clusters. Day et al. have shown that $Nb_2W_4O_{19}H^{3-}$ clusters react with siloxy compounds in a transesterification reaction to form silyl esters[10] (@-OH + $Si(OR)_4$ → $Si(OR)_3O$-@ + ROH). In our study the protonation of the niobotungstate clusters was carried out in an organic slurry of the surfactant/cluster salt with chloroacetic acid. The solubility of the surfactant salts in THF was lower than that of the tetrabutylammonium salts studied by Day et al. As a result, the protonation reaction proceeded more slowly. Nonetheless, chemical analysis showed that partial protonation of the metal oxide cluster was possible, even in the salt. The XRD patterns of the TEOS-treated samples did not differ significantly from those of the corresponding nonprotonated samples, and the crystallinity was only slightly greater. IR spectra showed a lower silicate content in these samples, analogously to the samples that had been exposed to ammonium ions.

Removal of the organic component from TEOS-treated samples was accomplished by calcination in air at 300−350 °C and by extraction with ethanolic HCl. The intensities of the C−H stretching and deformation

(33) Gobetto, R.; Harris, R. K.; Apperley, D. C. *J. Magn. Reson.* **1992**, *96*, 119.

(34) Gordon, A. J.; Ford, R. A. *The Chemist's Companion*; John Wiley & Sons: New York, 1972.

vibrations associated with the surfactant were used as gauges to monitor the elimination of the surfactant. The samples lost their crystallinity during these treatments, as is shown in the X-ray patterns (Figure 7d). Since the walls of these materials are much thinner than the walls in MCM-41, the structure is not as stable and collapses to an amorphous phase when it loses the support of the surfactant molecules. In the NH_4^+-treated samples most of the sharp reflections also disappeared after HCl extraction. However, a pair of very broad low angle peaks centered around 31 and 10 Å indicate that more order was maintained in these samples.

FTIR spectra showed that the HCl/EtOH extraction removes most of the template as well as ethyl groups associated with TEOS. Both, silicate groups and metal oxide clusters remained present after calcination or HCl/EtOH extraction. The intensity of the cluster absorptions decreased with respect to the Si–O absorption after extraction. This effect was smaller for NH_4^+-treated samples.

BET Analysis of Micro- and Mesoporosity. Nitrogen adsorption and desorption isotherms were obtained to determine the surface area and micro-/mesoporosity of the samples. With the surfactant present, the Si–Nb_2W_4 sample was nonporous (1–2 m^2/g). After partial removal of the template, the surface area increased by an order of magnitude, most of the new surface area originating from mesopores (>17 Å). For example, a surface area of 27 m^2/g was obtained after calcination of the Si–Nb_2W_4 sample, nearly all of the area due to pores with diameters exceeding 17 Å (mesopores). An HCl-extracted/NH_4^+-treated Si–Nb_2W_4 sample in which IR showed that some surfactant was still present displayed a surface area of 50 m^2/g (92% above 17 Å). Complete HCl extraction of Si–Nb_2W_4 resulted in a surface area of 221 m^2/g. In this case a significant fraction of micropores became accessible: 85% of this surface area pertained to pores smaller than 40 Å and 46% to pores smaller than 17 Å. It is notable that all Si–Nb_3W_3 samples exhibited a BET surface area of only 2–4 m^2/g, even after complete surfactant removal by acid extraction. The highest surface area of 265 m^2/g was observed for an HCl-extracted Si–Nb_4W_2 sample that had been treated with NH_4^+. 83% of this surface area was associated with pores smaller than 17 Å. The virtually glassy structure of the materials was thus composed of both mesopores and micropores. A particle size determination by TEM showed an average diameter of ca. 70 μm, indicating that the high surface area cannot be attributed to the size of small, dense spherical particles.

Conclusions

The salt–gel process has been used to connect prestructured cluster arrays. Weakly ordered porous structures with high surface areas were obtained after the surfactant template was removed from TEOS-treated niobotungstate salts by acid extraction. Double resonance NMR spectra show that Nb–O–Si linkages exist in these materials. FTIR and XRD data confirm that silicate was indeed incorporated in the salt structures and changed these structures.

The high surface areas are due to the composite niobotungstate/silicate network and cannot be due to physical mixtures of niobotungstate salt with silicate gel for several reasons. First, the through-space coupling of ^{93}Nb and ^{29}Si nuclei in the composite material is short range and could not be observed if these atoms were confined to separate solid phases. Second, if a mixture of a nonporous niobotungstate salt and a porous silicate gel were present, the surface area (based on the silicate content of the sample) of the gel would be in the range of 700 m^2/g. Such a surface area has been observed in silicate gels obtained by hydrolysis of TEOS.[29] However, none of the unextracted Si–Nb_xW_{6-x} salts had surface areas higher than 4 m^2/g. Thus, excess silicate gel cannot be responsible for the dramatic increase in surface area that was observed upon extraction of the surfactant from the niobotungstate structure. In addition, one would not expect the surface area of the extracted Si–Nb_3W_3 sample to be so much lower than that of the corresponding Si–Nb_2W_4 and Si–Nb_4W_2 samples, if mere physical mixtures were present.

The order, rigidity, and crystallinity of the porous products might be improved by using shorter templates (e.g., dodecyltrimethylammonium instead of cetyltrimethylammonium) for the cluster salts. Shorter templates are likely to bring the clusters closer together, thereby shortening the silicate connections between clusters, which impart elasticity to the structures.

The salt–gel method can probably be generalized and applied to other salt structures consisting of reactive ions or molecules that can be bridged. Its applicability to the synthesis of microporous and mesoporous materials will be explored further in future work.

Acknowledgment. We are grateful to Professor F. Cannon, Pennsylvania State University, for allowing us to use his BET equipment, to Dr. S. Hoyle and Professors D. K. Smith, and G. G. Johnson, Jr. (Materials Research Laboratory, PSU) for making available the powder diffraction simulation programs, and to John Turner, National Center for Electron Microscopy, Lawrence Berkeley Laboratory, for assistance with photographic reproductions. This work was supported by a grant (GM 43844) from the National Institutes of Health. Grateful acknowledgment is also extended to Nissei Sangyo America, Inc. for kindly providing a Hitachi H-9000NAR microscope to the University of California. Portions of the TEM work were carried out at the National Center for Electron Microscopy, Lawrence Berkeley Laboratory, a facility funded by the Director, Office of Energy Research, Office of Basic Energy Sciences, Materials Sciences Division of the U.S. Department of Energy under Contract Number DE-AC03-76SF00098. A.S. thanks the Natural Sciences and Engineering Research Council of Canada for a postdoctoral fellowship. T.E.M. thanks the Camille and Henry Dreyfus foundation for support in the form of a Teacher–Scholar Award. K.T.M. thanks the Camille and Henry Dreyfus foundation for support through a New Faculty Award.

CM940368T